The following publication Dean Yuan, Jiawei Luo, Daixuan Wu, Runsen Zhang, Puxiang Lai, Zhaohui Li, and Yuecheng Shen, "Single-shot ultrasound-modulated optical tomography with enhanced speckle contrast," Opt. Lett. 46, 3095-3098 (2021) is available at https://doi.org/10.1364/OL.425535.

Single-shot ultrasound-modulated optical tomography with enhanced speckle contrast

DEAN YUAN, [1†] JIAWEI LUO, [1†] DAIXUAN WU, [1] RUNSEN ZHANG, [2] PUXIANG LAI, [3,4,5] ZHAOHUI LI [1], AND YUECHENG SHEN [1,6]

[1]*Key Laboratory of Optoelectronic Materials and Technologies, School of Electronics and Information Technology, Sun Yat-sen University, Guangzhou 510275, China*
[2]*Guangdong Provincial Key Laboratory of Optical Fiber Sensing and Communications, Institute of Photonics Technology, Jinan University, Guangzhou 511443, China*
[3]*Department of Biomedical Engineering, Hong Kong Polytechnic University, Hong Kong SAR, China*
[4]*Shenzhen Research Institute, Hong Kong Polytechnic University, Shenzhen, China*
[5]puxiang.lai@polyu.edu.hk
[6]shenyuecheng@mail.sysu.edu.cn

Received XX Month XXXX; revised XX Month, XXXX; accepted XX Month XXXX; posted XX Month XXXX (Doc. ID XXXXX); published XX Month XXXX

Ultrasound-modulated optical tomography (UOT) images optical contrast deep inside biological tissue. Among existing approaches, camera-based parallel detection is beneficial in modulation depth but is limited to the relatively slow framerate of cameras. This condition prevents such scheme from achieving maturity to image live animals with sub-millisecond speckle correlation time. In this work, we developed on-axis single-shot UOT by investigating the statistics of speckles, breaking the restriction imposed by the slow camera framerate. As a proof of concept, we experimentally imaged a one-dimensional absorptive object buried inside a moving scattering medium with speckle correlation time down to 0.48 ms. We envision that this single-shot UOT is promising to cope with live animals with fast speckle decorrelation. © 2021 Optical Society of America

http://dx.doi.org/10.1364/OL.99.099999

Optical imaging of biological tissue reveals rich physiological information but optical scattering prevents imaging deeply [1]. To implement high-resolution optical imaging with abundant contrast at depths up to several centimeters, ultrasound-modulated optical tomography (UOT), also called acousto-optic imaging, was developed to image optical absorption with acoustic resolution and optical specificity. The principle behind UOT is the acousto-optic effect that tags a portion of photons passing through the focal region of the ultrasonic waves and induces a frequency shift equal to the ultrasonic frequency [2]. The number of tagged photons is determined by the local intensity of both light and ultrasound within the ultrasonic focal spot, which reflects the information of local optical properties at this position [3]. Due to this capability, UOT was recently demonstrated to image through the human skull [4] and was also combined with other optical imaging modalities to extend imaging depth [5, 6].

Since the acousto-optic effect is usually weak, one of the key challenges that UOT faces is how to detect weak tagged light overwhelmed by a huge background of untagged light. In the early years, single-pixel detectors, such as photodiodes [7] or photomultiplier tubes [8] were commonly used. These detectors can respond fast but suffer from insufficient modulation depth [9]. Although Fabry-Perot interferometers [10], spectral-hole burning [11], and laser cavity [12] were employed to filter untagged photons, these approaches require additional layout with special care. An alternative approach is to use pixel-array detectors like cameras to increase the modulation depth through parallel detection [13]. When the sizes of the camera pixels and the speckle grains are one-to-one mapped, it has been rigorously shown that the modulation depth can be increased by $\sqrt{N}$, where N is the number of speckles captured. Furthermore, a strong reference light was usually employed to balance the reduced photon flux due to the small sensor size, achieving shot-noise limited detection [14]. Recently, parallel detection was also extended to diffusing wave spectroscopy [15], enabling the measurement of blood flow in brains [16].

Although parallel detection with cameras is superior in terms of modulation depth, the framerate of cameras is usually slow. On-axis heterodyne holography requires a few camera-shots to retrieve optical field through phase shifting [17], making camera-based UOT challenging for *in vivo* applications with speckle correlation on the orders of sub-millisecond. In contrast, off-axis heterodyne holography enables the determination of optical field in a single-shot [18], but multiple camera pixels were required to sample one speckle grain, thereby scarifying the modulation depth in turn. Recently, we proposed to use a lock-in camera to measure optical field in a single-shot, but the state-of-the-art camera supports only 300 × 300 pixels [19]. Certain types of photorefractive crystals exhibit short response time while processing a large number of speckles [20-22]. However, these crystals only work for a narrow spectral range. Instead of beating speckle decorrelation, UOT also borrowed the concept of speckle contrast imaging to quantify ultrasound-induced blurring of speckle grains [23]. Despite the demonstrated performance, how to differentiate the decreased speckle contrast induced by the ultrasound and by other physiological motion remains challenging

[24]. Inspired by previous works on speckle contrast, we developed on-axis single-shot UOT in this work. In contrast to speckle contrast imaging that usually sets a long camera exposure time, we reduced the exposure time and intentionally designed an interferogram such that ultrasound considerably increased speckle contrast during a single camera exposure. Since the detection can be accomplished within a single shot and the exposure time can be conveniently reduced within 1 ms for modern cameras, we anticipate that the developed single-shot scheme holds promises for future *in vivo* applications.

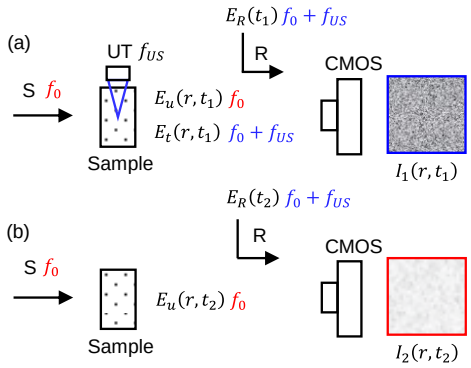

Fig. 1. Principle of on-axis single-shot UOT. S, sample beam; R, reference beam; UT, ultrasonic transducer; CMOS, scientific CMOS camera. (a) When the ultrasound is on, the speckle contrast increases due to the interference between the tagged light and the reference light. (b) When the ultrasound is off, no steady interference can be formed due to the frequency mismatch between the untagged light and the reference light.

We first describe the principle of on-axis single-shot UOT. As shown in Fig. 1(a), at time t_1, light with a frequency of f_0 illuminates the sample and the focused ultrasound with a frequency of f_{US} tags a portion of the light passing through the ultrasonic focus. In this condition, the transmitted scattered light can be divided into two parts: the untagged light $E_u(r,t_1)$ with the original frequency and the tagged light $E_t(r,t_1)$ with a frequency upshifted to $f_0 + f_{US}$ due to ultrasonic modulation. For simplicity, we omitted the downshifted part and higher-order terms of the tagged light. A reference light $E_R(t_1)$ with a frequency of $f_0 + f_{US}$ then interferes with the scattered light. The resulting camera-measured speckle distribution is

$$I_1(r,t_1) = |E_u(r,t_1)|^2 + |E_t(r,t_1)|^2 + |E_R(t_1)|^2 + 2|E_t(r,t_1)||E_R(t_1)|\cos\big(\varphi(r,t_1)\big) \quad (1)$$

Here, only the components with the same frequency contribute to the interference term and $\varphi(r,t_1)$ is the phase difference between the tagged light and the reference light. For conventional UOT, retrieving $|E_t(r,t_1)|$ requires additional measurement to remove the contaminations from $|E_u(r,t_1)|^2$. Thus, the camera needs to take another shot at time t_2 with ultrasound being switched off. At this time, the camera-measured speckle distribution is

$$I_2(r,t_2) = |E_u(r,t_2)|^2 + |E_R(t_2)|^2 \quad (2)$$

If $t_2 - t_1$ is within the speckle correlation time, then we have $|E_u(r,t_1)|^2 \approx |E_u(r,t_2)|^2$. Thus, subtracting Eq. (2) from Eq. (1) and neglecting $|E_t(r,t_1)|^2$ yields UOT signal

$$\mathrm{UOT}_{\mathrm{conv}} = \langle |I_1(r,t_1) - I_2(r,t_2)| \rangle \quad (3)$$

The operation $\langle\cdot\rangle$ denotes taking average concerning r. Two camera shots denote that the system latency is inevitably restricted by the framerate of the camera. However, the frame rates for cameras with high dynamic range are usually on the orders of several hundred, which are not fast enough to beat speckle decorrelation of live animals. This regretful situation prohibits camera-based UOT from being applied for in vivo studies. Notably, the intensity fluctuation of the speckles in Fig. 1(a) is considerably larger than that of the speckles in Fig. 1(b), owing to the interference term. This observation promotes us to think whether the enhanced intensity fluctuation of speckles can be used for UOT. Since the statistics of speckles does not change with fast speckle decorrelation, we found that by taking the standard deviation to $I_1(r,t_1)$ and $I_2(r,t_2)$ concerning r, the dependence on time can be removed. This observation indicates that this operation removes the restriction on the time interval between the two measurements. Thus, we can define

$$\mathrm{UOT}_{\mathrm{std}} = \sqrt{\mathrm{Std}^2(I_1(r,t_1)) - \mathrm{Std}^2(I_2(r,t_2))} \quad (4)$$

as the UOT signal. This value describes the variations in the intensity fluctuations of the speckles caused by the tagged light, which carries spatial information. Before proceeding, we emphasize that in contrast to conventional UOT, Eq. (4) allows a different metric, i.e., the standard deviation of intensity measurements, to quantify the ultrasonic modulation. Moreover, since Eq. (2) does not involve triggering ultrasound, $\mathrm{std}(I_2(r,t_2))$ can be estimated in prior and treated as a constant value throughout the experiment. Thus, by using Eq. (4), the UOT signal originated from the ultrasonic focus can now be estimated within a single shot, which is desirable for *in vivo* applications. When the tagged light becomes weak, we can neglect high-order terms of $|E_t(r,t_1)|$. Thus, both Eqs. (3) and (4) can be further simplified as

$$\mathrm{UOT}_{\mathrm{conv}} = \langle 2|E_t(r,t_1)||E_R(t_1)|\left|\cos\big(\varphi(r,t_1)\big)\right| \rangle \quad (5)$$

$$\mathrm{UOT}_{\mathrm{std}} = \sqrt{\langle 4|E_t(r,t_1)|^2|E_R(t_1)|^2\cos^2\big(\varphi(r,t_1)\big)\rangle} \quad (6)$$

The only difference between these two expressions is the switched order of square operation and spatial averaging. Thus, they represent the same physical quantity with different regulations (L1 and L2).

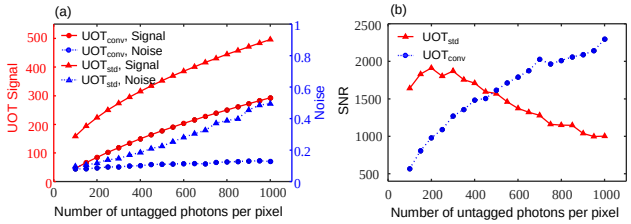

Fig. 2. Numerical results of on-axis single-shot UOT. (a) UOT signal and noise as a function of the number of untagged photons per pixel. (b) Signal-to-noise ratio as a function of the number of untagged photons per pixel.

The feasibility of the single-shot UOT was first examined using numerical tools. A self-written script written in Matlab was used to numerically estimate Eqs. (1)-(6) by statistical means. For computational convenience, each intensity term in these equations was translated using the representation of photon numbers. During the computational process, the dimension is set to be 2560 × 2160, matching with the resolution of the camera used in practice. For each unit, the number of photons for both tagged light and untagged light is drawn from the Rayleigh distribution, while the phase difference is drawn from a uniform distribution. To mimic practical conditions of imaging samples with different thicknesses, we

simulated various conditions by considering different numbers of untagged photons received at the detection plane. The strength of the ultrasound was fixed in this study for convenience so that the ratio between the number of tagged light and the untagged light at the detection plane is set to a fixed number of 0.5% [25]. The number of photons for the reference light at each unit is set to 20,000. Based on Eq. (4), the computed UOT_{std} as a function of the number of untagged photons is plotted in Fig. 1(a) using red triangles. As a comparison, the conventional UOT signal computed through Eq. (3) with two measurements is also plotted using red circles. Here, shot noise is considered but speckle decorrelation is not involved. For any measurement, the shot noise was simulated by picking a random number of a Poisson distribution, of which the total number of measured photons was set as the mean. These results denote both approaches can reconstruct UOT signals with roughly the same order, while UOT_{std} is slightly larger than UOT_{conv} The standard deviations of 100 independent measurements were plotted in blue in Fig. 2(a) as the noise level. Figure 2(b) plots the signal-to-noise ratio (SNR), showing that the SNR of UOT_{std} decreases when the number of untagged photons increases, due to the growing fluctuations of $|E_u(r,t_1)|^2$. In contrast, the SNR of UOT_{conv} increases along with the increased number of untagged photons, as the number of tagged photons also increases. Nonetheless, the SNR of UOT_{std} is larger than that of UOT_{conv} when the number of untagged photons is small, indicating UOT_{std} is suitable for thick biological tissue with a low photon budget. Since parallel detection with millions of pixels was employed and only shot noise was considered during simulation, the SNRs presented here are significantly higher than those found during experiments with a complicated condition.

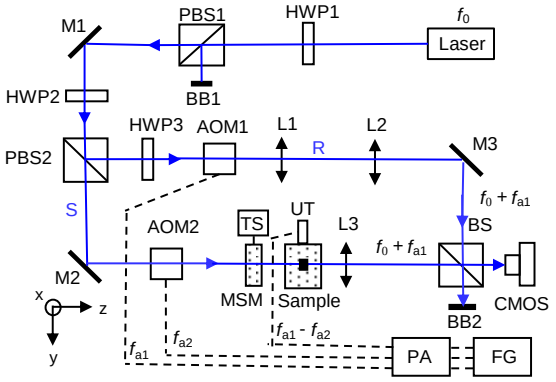

Fig. 3. Schematic diagram of the experimental setup for single-shot UOT. HWP, half-wave plate; PBS: polarizing beam splitter; BB, beam block; M, mirror; AOM, acousto-optic modulator; L, lens; TS, motorized translational stage; MSM, moving scattering medium; UT, ultrasonic transducer; CMOS, scientific CMOS camera; PA, power amplifier; FG, function generator; R, reference beam; S, sample beam.

Having described the principle of the single-shot UOT and discussed its performance numerically, we then built an experimental setup that is schematically shown in Fig. 3. The output of a 473-nm continuous-wave laser (MSL-FN-473-30mW, CNI) was chosen as the source, which was then split into a reference beam (R) and a sample beam (S). After passing through two acousto-optic modulators (AOM-505AF1, IntraAction), the frequencies of the reference beam and the sample beam were modulated to be $f_0 + f_{a1}$ and $f_0 + f_{a2}$, respectively, where f_{a1} = 52 MHz and f_{a2} = 47 MHz. Tissue-mimicking phantoms were made as scattering media, which were produced by mixing milk, gelatin, and water with a preset composition [26]. By choosing a mass ratio of 5:10:85 for milk, gelatin, and water, the scattering coefficient (μ_s) and reduced scattering coefficient (μ_s') were measured to be 7 mm^{-1} and 1 mm^{-1}, which is close to that of soft tissue at visible spectrum. The absorption of the phantom is negligible. To simulate different speckle decorrelation, a moving scattering medium (MSM, 45 mm × 45 mm × 1 mm) was mounted on a motorized translational stage (GCD-202050M, Daheng Optics, 0.37 mm/s-20 mm/s velocity, 50 mm travel range). Another scattering medium (36 mm × 36 mm × 2 mm) was placed 15 mm behind the MSM and an absorptive object (1.5 mm × 5 mm × 1 mm) made of gelatin and ink was placed on it. The absorption coefficient of this black target was quantified to be 5.3 mm^{-1}. A focused ultrasonic transducer (UT, ShanChao5Z10SJ30DJ; 5 MHz central frequency; 3 cm focal length; 0.918 mm focal spot size) was placed above the sample. When the sample beam illuminated the sample, the UT emitted ultrasound along the *y*-direction. Thus, the tagged light and the reference light shared the same frequency of $f_0 + f_{a1}$ and the interferogram was subsequently measured by a scientific CMOS camera (pco.edge 5.5, PCOTECH; 2,560 × 2,160 pixels; exposure time 0.5 ms).

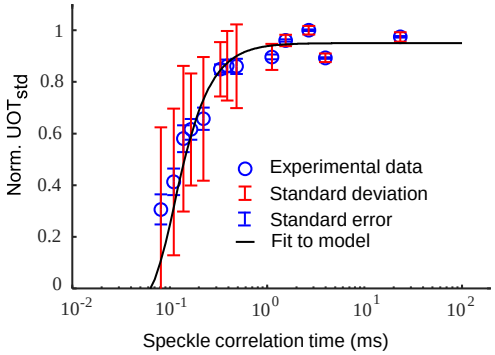

Fig. 4. Normalized UOT signal as a function of speckle correlation time. 30 independent measurements were used for generating each data point.

The first experiment we performed was to check whether ultrasound increases the intensity fluctuations of the speckles, i.e., the speckle contrast. A pulse train of ultrasound with 3000 cycles was generated for each firing process, resulting in a duration of 600 μs. The peak pressure at the focus was about 0.5 MPa, which is well below the damage threshold for biological tissues. The intensities of R and S were adjusted so that the average readings on the camera were 20,000 and 800, respectively. A series of 30 measurements were made with and without ultrasonic modulation for static scattering medium, and the standard deviations for these measured intensity patterns were computed. Quantitative results show that the averaged values for standard deviations with and without ultrasonic modulation were 2.77×10^3 and 2.57×10^3, respectively. These results confirm that speckles with ultrasonic modulation exhibit a considerably higher intensity fluctuation than speckles without ultrasonic modulation, confirming the validity of the developed approach. It is worth mentioning here that, this observation is completely different from the previous UOT that exploiting speckle contrast, wherein the speckle contrast with

ultrasonic modulation is lower than that without ultrasonic modulation [27].

Next, we investigated the performance of the setup in fighting against speckle decorrelation. The correlation time of speckles was controlled by translating the MSM along the *x*-axis at different speeds. Following the procedures developed in Ref. [19], a mathematical relationship $\tau_c = 1.63/v$ [ms] (the unit of v is mm/s) was established, allowing us to control the speckle correlation time by setting the translational speed. When the ultrasonic focus is away from the absorptive object, we measured speckle patterns and computed $\mathrm{UOT_{std}}$ (normalized to the maximum value) for various τ_c, as shown in Fig. 4. Each data point was averaged from 30 independent measurements. The standard deviations of these measurements denoted in red showed the fluctuations, while the standard errors denoted in blue represented how accurate mean values were estimated. As expected, $\mathrm{UOT_{std}}$ remains around a constant when τ_c is large and starts to decrease when τ_c approaches the camera exposure time (~0.5 ms). We also found that when τ_c is smaller than the camera exposure time, the errors increase accordingly due to the decreased speckle contrast captured by the camera. By fitting these data using $g(\tau) = \exp[-(\tau_s/\tau)^2]$ [28], the system latency τ_s is estimated as 0.11 ms. It worth emphasizing here that, for such a single-shot scheme, the system latency is only determined by the exposure time of the camera.

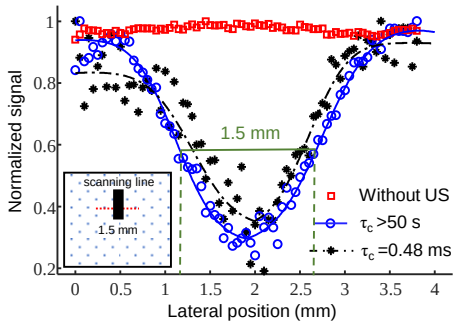

Fig. 5. One-dimensional image of an absorptive object buried inside scattering media. Each image is normalized by its maximum value. Blue circles: $\tau_c > 50$ s; black stars: $\tau_c = 0.48$ ms; red squares: direct transmission image. Each data point was generated through a single-shot measurement. Inset, schematics of the absorptive object. The fitting R^2 for the blue and black curves are 0.98 and 0.86, respectively.

Finally, we imaged a buried one-dimensional absorptive object (inset of Fig. 5) using the developed single-shot UOT. The ultrasonic focus was scanned at 0.05 mm per step along the *x* direction and $\mathrm{UOT_{std}}$ was estimated for each position. As shown in Fig. 5, the blue circles and the black stars represent data measured when $\tau_c > 50$ s and $\tau_c = 0.48$ ms, respectively. Both images manifested a dip located around the position of 1.9 mm, indicating the object. To quantitatively determine the lateral image resolution of the image, we fitted the experimental data with an imaging model: $y(x) = a\mathrm{erf}[2\sqrt{\ln 2}(x - x_1)/r_{\mathrm{FWHM}}] - b\mathrm{erf}[2\sqrt{\ln 2}(x - x_2)/r_{\mathrm{FWHM}}]$, where a, b, x_1, x_2 and r_{FWHM} are the fitting parameters while $\mathrm{erf}(x)$ is the error function [19]. The lateral resolutions r_{FWHM}, defined as the full-width at half maximum of the one-dimensional point spread function, were calculated to be 855.3 μm and 894.8 μm for $\tau_c > 50$ s and $\tau_c = 0.48$ ms, respectively. These values are consistent with the size of the ultrasonic focus (918 μm). As a comparison, Fig. 5 also shows the direct transmission image using red squares, obtained by collecting the total transmitted light at each scanning position when the ultrasonic transducer was off. These red squares exhibit a flat line, indicating that we could not identify the object buried inside without ultrasound modulation.

In conclusion, we developed on-axis single-shot UOT with enhanced speckle contrast. With this method, imaging an absorptive object buried inside scattering media with speckle correlation time down to 0.48 ms was demonstrated. Although 0.5-ms exposure time was employed throughout this study, a shorter exposure time could be used to further reduce the system latency at the expense of signal strength. It worth noting that further reducing exposure time down to nanosecond levels may cause the time-varying component in Eq. (1) not being easily averaged out, downgrading the effectiveness of this method. Nonetheless, such a phenomenon is not prominent for the current practice with microsecond exposure time. Therefore, the developed method holds promise for future imaging applications *in vivo*.

Funding. National Key Research and Development Program of China (2018YFB1802300); National Natural Science Foundation of China (12004446, 81930048); Guangdong Science and Technology Commission (2019A1515011374, 2019BT02X105).

Disclosures. The authors declare no conflicts of interest.

References

1. L. V. Wang, Dis. Mark. **19**, 123 (2003).
2. D. S. Elson, R. Li, C. Dunsby, R. Eckersley, and M.-X. Tang, Interface Focus **1**, 632 (2011).
3. P. Lai, R. A. Roy, and T. W. Murray, Opt. Lett. **34**, 2850 (2009).
4. Y. Liu, R. Cao, J. Xu, H. Ruan, and C. Yang, Opt. Lett. **45**, 2973 (2020).
5. M. Jang, H. Ko, J. H. Hong, W. K. Lee, J.-S. Lee, and W. Choi, Nat. Commun. **11**, 710 (2020).
6. H. Ruan, Y. Liu, J. Xu, Y. Huang, and C. Yang, Nat. Photonics **14**, 511 (2020).
7. M. Kempe, M. Larionov, D. Zaslavsky, and A. Z. Genack, J. Opt. Soc. Am. A **14**, 1151 (1997).
8. L. V. Wang, S. L. Jacques, and X. Zhao, Opt. Lett. **20**, 629 (1995).
9. S. G. Resink and G. Steffen, J. Biomed. Opt. **17**, 040901 (2012).
10. S. Sakadzic´, and L. V. Wang, Opt. Lett. **29**, 2770 (2004).
11. Y. Li, H. Zhang, C. Kim, K. H. Wagner, P. Hemmer, and L. V. Wang, Appl. Phys. Lett. **93**, 500 (2008).
12. K. Zhu, B. Zhou, Y. Lu, P. Lai, S. Zhang, and Y. Tan, Opt. Lett. **44**, 5414 (2019).
13. S. Lévêque, A. C. Boccara, M. Lebec, and H. Saint-Jalmes, Opt. Lett. **24**, 181 (1999).
14. M. Gross, P. Goy, and M. Al-Koussa, Opt. Lett. **28**, 2482 (2003).
15. J. Xu, A. K. Jahromi, and C. Yang, APL Photonics **6**, 016105 (2021).
16. J. Xu, A. K. Jahromi, J. Brake, J. E. Robinson, and C. Yang, APL Photonics **5**, 126102 (2020).
17. F. Le Clerc, L. Collot, and M. Gross, Opt. Lett. **25**, 716 (2000).
18. M. Gross, Appl. Opt. **56**, 1846 (2017).
19. Y. Liu, Y. Shen, C. Ma, J. Shi, and L. V. Wang, Appl. Phys. Lett. **108**, 231106 (2016).
20. T. W. Murray, L. Sui, G. Maguluri, R. A. Roy, A. Nieva, F. Blonigen, and C. A. DiMarzio, Opt. Lett. **29**, 2509 (2004).
21. M. Lesaffre, F. Jean, F. Ramaz, A. C. Boccara, M. Gross, P. Delaye, and G. Roosen, Opt. Express **15**, 1030 (2007).
22. B. Jayet, J. P. Huignard, and F. Ramaz, Opt. Lett. **38**, 1256 (2013).
23. J. Li, G. Ku, and L. V. Wang, Appl. Opt. **41**, 6030 (2002).
24. A. Hussain, W. Steenbergen, and I. M. Vellekoop, J. Biophotonics **11**, 1 (2018).

25. Y. Huang, M. Cua, J. Brake, Y. Liu, and C. Yang, J. Biomed. Opt. **25**, 025002 (2020).
26. P. Lai, X. Xu, and L. V. Wang, J. Biomed. Opt. **19**, 035002 (2014).
27. J. Li, S. Sakadzic´, G. Ku, and L. V. Wang, Appl. Opt. **42**, 4088 (2003).
28. D. D. Duncan, and S. J. Kirkpatrick, J. Opt. Soc. Am. A **25**, 2088 (2008).

References

1. L. V. Wang, "Ultrasound-mediated biophotonic imaging: a review of acousto-optical tomography and photo-acoustic tomography," Disease Markers **19**, 123-138 (2003).
2. D. S. Elson, R. Li, C. Dunsby, R. Eckersley, and M. X. Tang, "Ultrasound-mediated optical tomography: a review of current methods," Interface Focus **1**, 632-648 (2011).
3. P. Lai, R. A. Roy, and T. W. Murray, "Quantitative characterization of turbid media using pressure contrast acousto-optic imaging," Opt. Lett. **34**, 2850-2852 (2009).
4. Y. Liu, R. Cao, J. Xu, H. Ruan, and C. Yang, "Imaging through highly scattering human skulls with ultrasound-modulated optical tomography," Opt. Lett. **45**, 2973-2976 (2020).
5. M. Jang, H. Ko, J. H. Hong, W. K. Lee, J.-S. Lee, and W. Choi, "Deep tissue space-gated microscopy via acousto-optic interaction," Nature Communications **11**, 710 (2020).
6. H. Ruan, Y. Liu, J. Xu, Y. Huang, and C. Yang, "Fluorescence imaging through dynamic scattering media with speckle-encoded ultrasound-modulated light correlation," Nature Photonics **14**, 511-516 (2020).
7. M. Kempe, M. Larionov, D. Zaslavsky, and A. Z. Genack, "Acousto-optic tomography with multiply scattered light," Journal of the Optical Society of America A **14**, 1151-1158 (1997).
8. L. Wang, S. L. Jacques, and X. Zhao, "Continuous-wave ultrasonic modulation of scattered laser light to image object in turbid media," Opt. Lett. **20**, 629-631 (1995).
9. S. G. Resink, A. C. Boccara, and W. Steenbergen, "State-of-the art of acousto-optic sensing and imaging of turbid media," Journal of Biomedical Optics **17**, 040901 (2012).
10. S. Sakadžić and L. V. Wang, "High-resolution ultrasound-modulated optical tomography in biological tissues," Opt. Lett. **29**, 2770-2772 (2004).
11. Y. Li, H. Zhang, C. Kim, K. H. Wagner, P. Hemmer, and L. V. Wang, "Pulsed ultrasound-modulated optical tomography using spectral-hole burning as a narrowband spectral filter," Applied Physics Letters **93**, 500 (2008).
12. K. Zhu, B. Zhou, Y. Lu, P. Lai, S. Zhang, and Y. Tan, "Ultrasound-modulated laser feedback tomography in the reflective mode," Opt. Lett. **44**, 5414-5417 (2019).
13. S. Lévêque, A. C. Boccara, M. Lebec, and H. Saint-Jalmes, "Ultrasonic tagging of photon paths in scattering media: parallel speckle modulation processing," Opt. Lett. **24**, 181-183 (1999).
14. M. Gross, P. Goy, and M. Al-Koussa, "Shot-noise detection of ultrasound-tagged photons in ultrasound-modulated optical imaging," Opt. Lett. **28**, 2482-2484 (2003).
15. J. Xu, A. K. Jahromi, and C. Yang, "Diffusing wave spectroscopy: A unified treatment on temporal sampling and speckle ensemble methods," APL Photonics **6**, 016105 (2021).
16. J. Xu, A. K. Jahromi, J. Brake, J. E. Robinson, and C. Yang, "Interferometric speckle visibility spectroscopy (ISVS) for human cerebral blood flow monitoring," APL Photonics **5**, 126102 (2020).
17. F. Le Clerc, L. Collot, and M. Gross, "Numerical heterodyne holography with two-dimensional photodetector arrays," Opt. Lett. **25**, 716-718 (2000).
18. M. Gross, "Selection of the tagged photons by off axis heterodyne holography in ultrasound-modulated optical tomography," Appl. Opt. **56**, 1846-1854 (2017).
19. Y. Liu, Y. Shen, C. Ma, J. Shi, and L. V. Wang, "Lock-in camera based heterodyne holography for ultrasound-modulated optical tomography inside dynamic scattering media," Applied Physics Letters **108**, 231106 (2016).
20. T. W. Murray, L. Sui, G. Maguluri, R. A. Roy, A. Nieva, F. Blonigen, and C. A. DiMarzio, "Detection of ultrasound-modulated photons in diffuse media using the photorefractive effect," Opt. Lett. **29**, 2509-2511 (2004).
21. M. Lesaffre, F. Jean, F. Ramaz, A. C. Boccara, M. Gross, P. Delaye, and G. Roosen, "In situ monitoring of the photorefractive response time in a self-adaptive wavefront holography setup developed for acousto-optic imaging," Opt. Express **15**, 1030-1042 (2007).
22. B. Jayet, J. P. Huignard, and F. Ramaz, "Optical phase conjugation in Nd:YVO4 for acousto-optic detection in scattering media," Opt. Lett. **38**, 1256-1258 (2013).
23. J. Li, G. Ku, and L. V. Wang, "Ultrasound-modulated optical tomography of biological

tissue by use of contrast of laser speckles," Appl. Opt. **41**, 6030-6035 (2002).
24. A. Hussain, W. Steenbergen, and I. M. Vellekoop, "Imaging blood flow inside highly scattering media using ultrasound modulated optical tomography," Journal of Biophotonics **11**(2018).
25. Y. Huang, M. Cua, J. Brake, Y. Liu, and C. Yang, "Investigating ultrasound–light interaction in scattering media," Journal of Biomedical Optics **25**, 025002 (2020).
26. P. Lai, X. Xu, and L. V. Wang, "Dependence of optical scattering from Intralipid in gelatin-gel based tissue-mimicking phantoms on mixing temperature and time," Journal of Biomedical Optics **19**, 035002 (2014).
27. J. Li, S. Sakadžić, G. Ku, and L. V. Wang, "Transmission- and side-detection configurations in ultrasound-modulated optical tomography of thick biological tissues," Appl. Opt. **42**, 4088-4094 (2003).
28. D. D. Duncan and S. J. Kirkpatrick, "Can laser speckle flowmetry be made a quantitative tool?," J. Opt. Soc. Am. A **25**, 2088-2094 (2008).